**9th AIAA Aviation Technology, Integration, and Operations Conference (ATIO)
and
Air**
21 - 23 September 2009, Hilton Head, South Carolina

AIAA 2009-6909

Speed Control for Airborne Separation Assistance in Continuous Descent Arrivals

Eri Itoh[1],
Electronic Navigation Research Institute (ENRI), Chofu, Tokyo 182-0012, Japan

Mariken Everdij[2], Bert Bakker[3],
National Aerospace Laboratory NLR, 1059 CM Amsterdam, The Netherlands

and

Henk Blom[4]
National Aerospace Laboratory NLR, 1059 CM Amsterdam, The Netherlands

Airborne Separation Assistance System (ASAS) is seen as a promising option for the future ATM concept to increase capacity and flight efficiency while maintaining flight safety. One idea of recent interest in ASAS applications is Airborne SPacing Application using enhanced Sequencing and Merging (ASPA-S&M). The S&M is expected to support energy saving arrivals, commonly referred to as Continuous Descent Arrivals (CDA). The motivation for our study is the need to clarify how safety and capacity depend on the setting of spacing criteria and in combination with specific S&M design aspects, and to identify any potential emergent behavior that should be taken into account in the operation design. For this purpose, a preceding study has designed initial mathematical models of the ASAS application for two aircraft trailing. This research develops the models to multiple aircraft trailing under stochastic wind conditions. In this paper, ASAS core components and their interactions are captured to build an integrated model using a Stochastically and Dynamically Colored Petri Net (SDCPN). Through Monte Carlo simulation based on the SDCPN model, we evaluate the performance of ASAS speed control for CDA operation considering the wind effect and multiple trailing aircraft.

Nomenclature

ASAS spacing controller (Section II. A)

K_I	= integral gain
K_P	= loop closure gain
s	= Laplace transform
ω_{man}	= maneuver bandwidth
ζ_{man}	= maneuver damping
$V_{cmd_{TAS}}$	= TAS command given to autopilot
$V_{max_{TAS}}$	= maximum value of True Air Speed (TAS)

---

[1] Research Scientist, PhD, Air Traffic Management Department, 7-42-23, Jindaiji-higashi, Chofu, Tokyo 182-0012, Japan.

[2] Senior Scientist, NLR Air Transport Safety Institute, Anthony Fokkerweg 2, 1059 CM Amsterdam, The Netherlands.

[3] Stochastic Analyst, NLR Air Transport Safety Institute, Anthony Fokkerweg 2, 1059 CM Amsterdam, The Netherlands.

[4] Principal Scientist, PhD, NLR Air Transport Safety Institute, Anthony Fokkerweg 2, 1059 CM Amsterdam, The Netherlands.

$V_{min\,TAS}$ = minimum value of TAS
ε_v = upper limit of Ground Speed (GS) difference
$\varepsilon_{\dot{v}}$ = upper limit of the derivative of GS difference
$\varepsilon_{\dot{v}_{cmd}}$ = upper limit of the derivative of $V_{cmd\,TAS}$
ε_{vyr} = lower limit of the ratio of GS difference and y_{error}
ε_y = upper limit of y_{error}

Stochastic atmospheric condition (Section II. B)

a_1 = constant number
a_2 = constant number
L_u, L_v, L_w = scale length corresponding to x, y, z axes
U = mean wind speed at 10 m. (unit: m/s)
$\sigma_u,\ \sigma_v,\ \sigma_w$ = root mean square (rms) turbulence intensity corresponding to x, y, z axes
ω_m = mean wind at altitude h meters ($h \geq 1$ m)
ω_{tu} = turbulence following the x direction of the body axis.
ω_{tv} = turbulence following the y direction of the body axis
ω_{tw} = turbulence following the z direction of the body axis

Monte Carlo simulation (Section IV)

c = indicator of separation loss events
f_N = normal distribution
f_U = uniform distribution
h_{enter}^{max} = maximum entrance attitude
h_{enter}^{min} = minimum entrance attitude
h_{ini} = initial attitude
p = provability of separation loss
$V_{CAS_{ini}}$ = initial Calibrated Air Speed (CAS)
V_{enter} = entrance CAS
w = weight given to particle
σ_V = distribution of entrance CAS
γ = fraction given by Interacting Particle System (IPS) approach

I. Introduction

Airborne Separation Assistance System (ASAS) is an integrated air to air, and air to ground system which enables flight crews to maintain airborne separation by visualizing surrounding air traffic information in a cockpit display. It allows shifting Air Traffic Controller (ATCo)'s tasks to the crew during flight. One idea of recent interest in ASAS applications is Airborne SPacing Application using enhanced Sequencing and Merging (ASPA-S&M) [1]. This application asks the crew to achieve and maintain a given time-spacing to the target aircraft at a chosen waypoint. The S&M is expected to support energy saving arrivals, commonly referred as Continuous Descent Arrivals (CDA). The questions are how safety and capacity depend on the setting of spacing criteria and in combination with specific S&M design aspects, and to identify any potential emergent behavior that should be taken into account in the operation design. The motivation for our study is the need to properly understand the nominal and non-nominal behavior of many aircraft when the S&M is applied. The state of the art in scientific research is that non-nominal emergent behavior of advanced designs can be identified through conducting large scale Monte Carlo simulations with a well specified multi-agent based mathematical model of the operation [2]. In line with this, this research furthers the mathematical modeling and Monte Carlo simulation study for the S&M operation under the international research collaboration.

A preceding study [3] has designed initial mathematical models of the ASAS time-based spacing operation for two aircraft trailing. Current study improves the past work on the following three points: 1) a new ASAS spacing controller, which is developed in Ref. 4 to behave in a much more robust way, is applied to the model. 2) Stochastic atmospheric conditions (wind and turbulence) are included in the model. 3) Multiple trailing aircraft (more than the two trailing aircraft) are considered. Additionally, this research changes the approach to handling the complexity in the modeling process. The preceding study [3] has designed ASAS including not only ASAS automatic guidance, but also Airborne Collision Avoidance System (ACAS), ATCo, pilot, data link, human-machine interaction, and rare

events as hardware failure, etc., in order to mimic the realistic system. On the other hand, this research firstly makes a simple ASAS core model, then increases the other component models in stages aiming to clarify interactions between them. As a first step, we build an ASAS automatic guidance model and evaluate its performance under CDA operation considering the wind effect and multiple aircraft trailing. This paper aims to clarify the following two questions: 1) does the comparative speed control in ASAS, which controls airborne time separation using position/airspeed errors between a target and a trailing aircraft, contribute to CDA operation? 2) does the ASAS speed control contribute for multiple aircraft to maintain the desired aircraft time separation in in-trail following?

For the mathematical modeling, the many components and their interactions that play roles in ASAS control loop have to be captured in an integrated model. When the airborne separation works without any intervention of the crew and neither of Air Traffic Controller (ATCo), the ASAS control loop consists of Guidance, Navigation, Control (GNC), and a Global Navigation Satellite System (GNSS). The guidance system contains the dynamics of aircraft, Flight Management System (FMS), autopilot, and control systems. The positioning system consists of a GPS receiver and sensors with probability distributions of position/velocity error. The communication system represents an ADS-B transmitter/receiver. The GNSS system contains the GPS performance. The desired airborne separation is achieved by the combination of spacing and surveillance. The ASAS control loop is a complex system in which these components stochastically and dynamically work and interact with each other. In order to handle the complexity of this modeling challenge well, we make use of a suitable Petri net formalism, a Stochastically and Dynamically Colored Petri Net (SDCPN)[5, 6]. The SDCPN is an extension of a Petri net which enables us to represent a system including stochastic behaviors and dynamic processes such that the resulting process model satisfies strong Markov property. The compositionally specified SDCPN models enable a systematic implementation of the complex system in computer programming for Monte Carlo simulation. The probabilities of separation loss events are estimated under the assumed performance of the ASAS components, desired capacity and flight conditions. For efficient computation, we use the Interacting Particle System (IPS) approach which speeds up the Monte Carlo simulation[7]. The IPS takes benefit of the fact that the specified SDCPN, stochastic process model, satisfies the strong Markov property.

This paper is organized as follows. In section II, the improvements over the past study[3], the designed ASAS spacing controller[4] and atmospheric model, are shown. In section III, ASAS components and their interactions under a defined CDA operation are modeled using the SDCPN. In section IV, the performance of the ASAS automatic guidance is evaluated using IPS approach. Stochastic wind behaviors, deviations of initial altitude and airspeed of the multiple aircraft are considered to count separation loss events in the Monte Carlo simulations. The simulation results show the performance of the ASAS speed control comparing with the case that the ASAS control does not work, and increasing the number of the trailing aircraft. In section V, it is explained how the results obtained in this paper are related to the ones in Ref. 3. Future works are indicated at the end.

II. Novel ASAS Spacing Control

A. ASAS Spacing controller
In support of Eurocontrol's CoSpace project[9], a conventional control law for ASAS spacing was developed[8] and this has been shown to work well under nominal conditions. Recently this control law has been significantly improved[4] regarding robustness against random deviations, for example, sudden wind changes, and deviations of initial aircraft speed and altitude.

One of the key design aspects of this novel controller is that it makes use of differences in ground speed rather than the conventional approach using differences in TAS. In the novel ASAS spacing controller, the CAS command, $V_{cmd\,CAS}$, is given by using the predicted position $y_{error\,GS}$. $y_{error\,GS}$ is based on its current position of the own (trailing), y_{own}, and lead (target) aircraft, y_{lead}, and Ground Speed (GS) of the own aircraft, $V_{own\,GS}$.

$$y_{error\,GS} = y_{lead} - y_{own} - separation_{time} \cdot V_{own\,GS} \tag{1}$$

$separation_{time}$ is a given time separation between a lead and own aircraft. This paper defines 90 seconds separation. Using Eq. (1), $V_{cmd\,CAS}$ is given as follows.

$$V_{cmd\,CAS} = K_P \cdot \left[y_{error\,GS} \cdot \omega_{man}^2 + \left\{ \frac{s + 2\zeta_{man}\,\omega_{man}}{\tau \cdot s + 1} \left(V_{lead\,GS} - V_{own\,GS} \right) \right\} \right] \cdot \frac{(K_I + s)}{s} \tag{2}$$

All parameter values of loop closure gain, K_P, maneuver band width, ω_{man}, maneuver damping, ζ_{man}, integral gain K_I, are given in Ref. 4 and 8. s is Laplace transform.

The other key in the novel design is that it increases the robustness against the initial deviation in airspeed and altitude[4]. The conventional ASAS spacing controller[8] had not been designed to cope with variations in initial conditions (i.e. airspeed, altitude, or separation errors at the time of engagement of the controller). Ref. 4 has added this capability to the controller by the following new constraints.

$$\left| y_{error_{GS}} \right| \leq \varepsilon_y \tag{3}$$

$$\left| V_{lead_{GS}} - V_{own_{GS}} \right| \leq \varepsilon_v \tag{4}$$

$$\left| d\left(V_{lead_{GS}} - V_{own_{GS}} \right)/dt \right| \leq \varepsilon_{\dot{v}} \tag{5}$$

$$\left| \left(V_{lead_{GS}} - V_{own_{GS}} \right)/y_{error\ GS} \right| \geq \varepsilon_{vyr} \tag{6}$$

$$V_{min\ TAS} \leq V_{cmd\ TAS} \leq V_{max\ TAS} \tag{7}$$

$$\left| dV_{cmd\ TAS}/dt \right| \leq \varepsilon_{\dot{v}_{cmd}} \tag{8}$$

All parameter values of upper limit of y_{error}, ε_y, upper limit of GS difference, ε_v, upper limit of the derivative of GS difference, $\varepsilon_{\dot{v}}$, lower limit of the ratio of GS difference and y_{error}, ε_{vyr}, minimum value of TAS, $V_{min\ TAS}$, TAS command given to autopilot, $V_{cmd\ TAS}$, maximum value of TAS, $V_{max\ TAS}$, and upper limit of the derivative of $V_{cmd\ TAS}$, $\varepsilon_{\dot{v}_{cmd}}$, are given in Ref. 4.

In Ref. 4, it has been shown that this novel controller has significant advantages over the conventional one of Ref. 3.

B. Stochastic atmospheric condition

Based on Ref. 10 and 11, stochastic atmospheric condition is modeled as the sum of the mean wind and turbulence.

Mean wind ω_m [10]

$$\omega_m = a_1 U log_{10}(h) + a_2 U \tag{9}$$

All values of parameters, mean wind at altitude h meters ($h \geq 1$ m), ω_m, mean wind speed at 10 m. (unit: m/s), U, constant number, a_1 and a_2 are given in Ref. 10.

Turbulence ω_{tu}, ω_{tv}, ω_{tw} [11]

Here turbulence following the x direction of the body axis, ω_{tu}, turbulence following the y direction of the body axis, ω_{tv}, and turbulence following the z direction of the body axis, ω_{tw}, are represented by Gaussian process passed through transfer functions, $H_u(s), H_v(s), H_w(s)$:

$$H_u(s) = \sigma_u \sqrt{\frac{2L_u}{\pi V}} \frac{1}{1 + \frac{L_u}{V}s} \tag{10}$$

$$H_v(s) = \sigma_v \sqrt{\frac{L_v}{\pi V}} \frac{1 + \frac{\sqrt{3}L_v}{V}s}{\left(1 + \frac{L_v}{V}s\right)^2} \tag{11}$$

$$H_w(s) = \sigma_w \sqrt{\frac{L_w}{\pi V}} \frac{1 + \frac{\sqrt{3}L_w}{V}s}{\left(1 + \frac{L_w}{V}s\right)^2} \tag{12}$$

All values of the parameters, root mean square (rms) turbulence intensity corresponding to x, y, z axes, σ_u, σ_v, σ_w, and scale length corresponding to x, y, z axes, L_u, L_v, L_w are given in Ref. 11.

Using Gaussian white noise w_g, $\omega_{tu}, \omega_{tv}, \omega_{tw}$ are:

$$\omega_{tu} = H_u(s)w_g \tag{13}$$

$$\omega_{tv} = H_v(s)w_g \tag{14}$$

$$\omega_{tw} = H_w(s)w_g \tag{15}$$

Figure 1 shows the wind speed given by the models.
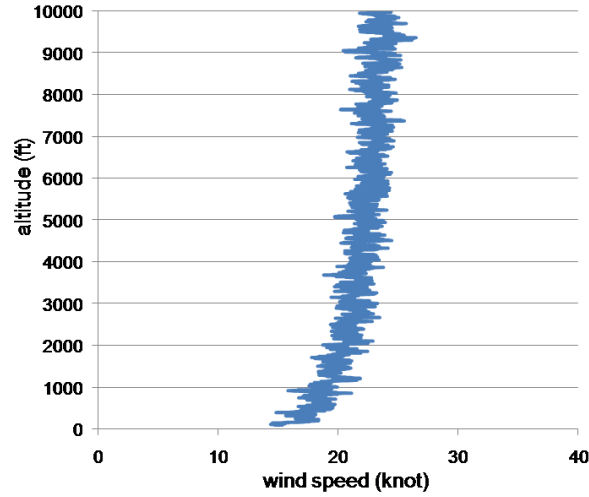

Fig. 1 Example for the wind speed model

III. Agent Level Petri Nets

In order to handle the complexity of the real system in the modeling, we employ the hierarchical way of working to develop the model. Firstly, at the top level agents are defined, and secondly, interactions between these agents are pictured. Thirdly, each agent is modeled in further detail in several local models and their local interactions.

Figure 2 shows the agents and their interactions in the ASAS control loop without any intervention of the crew and neither of Air Traffic Controller (ATCo). As shown in Fig. 2, each aircraft contains Aircraft evolution, Guidance systems, Own positioning systems, Communication systems, and ASAS agents. Own positioning systems takes satellite-based information from GNSS agent. Each aircraft transmits/receives the other aircraft information via Communication systems. Weather influences to the Guidance systems. In order to focus on the effect of the ASAS speed control in CDA, this paper gives following assumptions in the above agents: 1) Own positioning, Communication, GNSS systems work without any failure, corruption and degradation. 2) Position/velocity errors in Own positioning systems are assumed to zero. The above ASAS agents consist of detailed local models as follows.
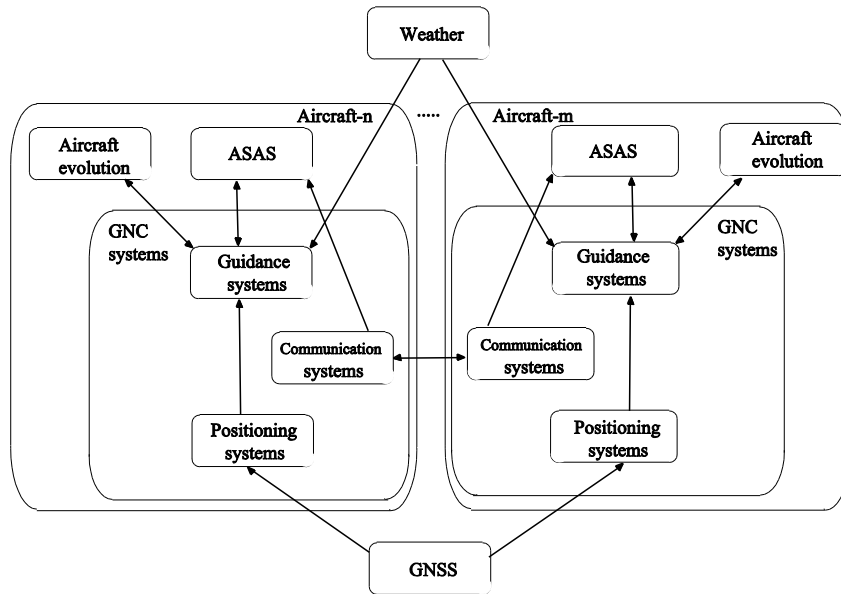

Fig.2 Multiple agents and their interaction

Aircraft evolution agent
- **Aircraft evolution model**

This shows the evolution of the aircraft that executes ASAS spacing.

Guidance systems agent
- **FMS (Flight Management System) flight plan model**

This describes the nominal flight plan of the aircraft.
- **Aircraft guidance behavior model**

This includes the dynamics of the aircraft including FMS, autopilot, and control systems. Initial values of aircraft speed and altitude are given by probability distributions.

Own positioning systems agent
- **Aircraft GPS receiver model**

This includes a probability distribution which describes the time intervals in which the aircraft's GPS receiver is working/not working.
- **Aircraft air sensor model**

This includes a probability distribution which describes the time interval in which the estimation of vertical aircraft position and speed is working correctly/degraded.
- **Aircraft horizontal POS-PROC model**

This describes the estimation error of two dimensional horizontal positions and speed of aircraft in GPS/IRS estimates. Probability distributions and dynamics are given for position/velocity errors.
- **Aircraft air data PROC model**

This describes the estimation errors of vertical position and speed, as well as the airspeed of the aircraft. The estimation of True AirSpeed (TAS) uses altitude estimated by altimeter and pitot tube measurement. Probability distributions and dynamics are given to estimate position/velocity error in altimeter/TAS measurement.

Communication systems agent
- **ADS-B transmitter model**

This includes a probability distribution which describes the time interval in which the aircraft's ADS-B transmitter is working/not working.
- **ADS-B receiver model**

This includes a probability distribution which describes the time interval in which the aircraft's ADS-B receiver is working/not working.

ASAS agent
- **ASAS spacing model**

Dynamics of ASAS space keeping controller, which automatically guides aircraft to keep certain time separation with a target aircraft, is given by ASAS time-based spacing criteria[4,8].
- **ASAS surveillance model**

This describes ADS-B information of all other aircraft in the ADS-B range, which the own aircraft updates every 1 second.

Global Navigation Satellite System (GNSS) agent
- **GPS system model**

This describes the time interval in which GPS is working/degraded/corrupted/down using a probability distribution.

Weather agent
- **Wind model**

This describes wind dynamics on 3 axis (x, y, z on the earth axis) as a combination of mean wind and disturbance which depends on altitude and air speed.

For the mathematical modeling of the above local models and interactions, we make use of a suitable Petri net formalism, Stochastically and Dynamically Colored Petri Net (SDCPN)[5, 6]. The SDCPN is a Petri net extension which allows representing a complex system including stochastic behaviors and dynamic processes. A Petri net is a graph of circles (named places), rectangles (named transitions) and arrows (named arcs). The places represent possible discrete modes or conditions, the transitions represent possible actions. The arcs exist between places and transition or vice versa. A condition is current if a token (represented by a dot) is residing in the corresponding place. One of the powerful advantages of Petri nets includes their graphical representation to model a complex system in all of its components and their interactions. In an SDCPN model, each token is associated with differential equation which represents the dynamic process in the applied system. The SDCPN models which take important roles in ASAS speed control, Aircraft guidance behavior and ASAS spacing model are introduced in Appendix C and D.

IV. Simulation results of ASAS Speed Control

In this section we perform Monte Carlo simulations for ASAS speed control for use within CDA. In Subsection IV.B, we consider a pair of aircraft. Next, in subsection IV.C, we consider a string of multiple aircraft. Prior to looking at these two subsections, in subsection IV.A we first explain the specific approach that we use in running Monte Carlo simulations for these scenarios.

A. Accelerating the Monte Carlo simulation

For the performance evaluation of the ASAS speed control in CDA operation, the probabilities of aircraft separation loss events are estimated over the designed SDCPN model using Monte Carlo simulation that is accelerated using an importance sampling approach which is referred to as Interacting particle System (IPS).

The basic idea of Monte Carlo simulation is straightforward. Define N as the number of sample simulated operations, and c_i the indicator of separation loss events for the sample i:

$$c_i = \begin{cases} 0 & \text{if sample } i \text{ does not lose defined separation} \\ 1 & \text{if sample } i \text{ loses defined separation} \end{cases}$$

If all sampled operations have the same weight, then the estimated probability of the separation loss event p is

$$p = \frac{1}{N} \sum_{i=1}^{N} c_i \tag{16}$$

In the case we count the collision risk, the probability p is expected to be as low as $10\exp-9$. Then the number of simulated samples necessary for the Monte Carlo returning valid results (i. e., a non-zero result), would be expected to be of order of $10\exp11$, and Ref. 3 estimates that without acceleration, the computing time might take 1,500 years. In order to avoid this, appropriate techniques have to be used to speed up Monte Carlo simulations. The technique we use for the speed up of Monte Carlo simulation is the IPS approach[7]. The same acceleration approach has successfully been used in Ref. 3. The IPS takes benefit of the fact that the probabilities of sequence events on aircraft separation loss constitute realizations of a strong Markov process: the probability that an aircraft loses separation in the future time interval is higher for aircraft that already have smaller separation distance at present time. In the IPS approach, the following four steps are iterated:

Step 1. A number $l = 1, \cdots, N$ of samples (particles) simulate a new path of the hybrid state Markov process until the next separation loss event k or the end of the simulation time.

Step 2. If the separation loss events of the particles are counted in Step 1, fraction γ_k which is the conditional probability of reaching the next separation loss event is assessed by summation of weights given to the counted particles, w_k^l.

Step 3. The particles which reach the separation loss events are stored. The other particles are deleted.

Step 4. Draw N particles by randomly copying the stored particles in Step 3. Each of particles gets a weight, w_{k+1}^l.

Reference 7 provides further details of this IPS cycle. Table 1 specifies the sequence of events that have been used in the IPS based Monte Carlo simulations in this paper.

Table 1 Separation levels and events

Level of Separation loss events	Horizontal separation distance (NM)	Vertical separation distance (ft)	Separation loss event
1	6.0	1,500	-
2	4.5	900	Minimum Separation Infringement, Europe (MSI #1) [3]
2.1	3.5	800	-
2.2	3.25	750	-
3	3.0	700	Minimum Separation Infringement, Japan (MSI #2)
4	1.25	500	Near Mid-Air Collision (NMAC)
5	0.03	52.5	Mid-Air Collision (MAC)

B. ASAS Speed Control in CDA

In this section, the performance of the ASAS speed control in CDA operation is compared to the performance without the ASAS speed control for one pair of trailing aircraft.

Firstly, we simulate the situation that two aircraft conduct CDA operation under the head-wind condition (Section II. B). A first aircraft enters Initial Approach Fix (IAF), then continuously descends to the Final Approach Fix (FAF) by keeping a 2.5 degree flight path and the initial airspeed. After reaching the FAF at 2,000 ft, the aircraft reduces airspeed to 180 CAS knots and increases the flap angle to 25 degrees proportionally for 100 seconds. The distance between IAF and FAF is 45.0 NM. The second aircraft enters IAF 90 seconds after the first aircraft. The B747-400 dynamics are given to the two aircraft by AMAAI tool box[8]. We use a computing time step of 0.1 second.

Here we consider probability distributions of initial altitude, h_{ini} , and initial CAS, $V_{CAS_{ini}}$, at IAF. When $\xi \leftarrow f(x; \ \mu)$ denotes that the value $\xi \in \mathbf{R}$ is drawn from the probability density function $f(x; \ \mu)$ where μ is one or more parameters, h_{ini} and $V_{CAS_{ini}}$ are given as follows.

$$h_{ini} \quad \leftarrow \quad f_U(x; h_{enter}^{min}, \quad h_{enter}^{max}) \tag{17}$$

$$V_{CAS_{ini}} \quad \leftarrow \quad f_N(x; V_{enter}, \quad \sigma_V) \tag{18}$$

Table 2 Parameter settings in initial values

Parameter	Value
h_{enter}^{min}	10,000 (ft)
h_{enter}^{max}	11,000 (ft)
V_{enter}	240 (knot)
σ_V	5 (knot)

Table 2 shows the parameter settings in Eqs. (17) and (18). The uniform density $f_U(x; \ l, \ u)$ and normal density $f_N(x; \ \mu, \ \sigma)$ are defined respectively:

$$f_U(x; \ l, \ u) = \begin{cases} \frac{1}{u-l} & l \leq x \leq u \\ 0 & else \end{cases} \tag{19}$$

$$f_N(x; \ \mu, \ \sigma) = \frac{1}{\sqrt{2\pi}\sigma} exp\left(-\frac{(x-\mu)^2}{2\sigma^2}\right) \tag{20}$$

By running ten times the IPS algorithm, the risk of the separation loss event is estimated. The number of particles per IPS simulation run is 10,000. For the ten IPS runs, the estimated fractions γ_k are given in Table 3 for each of the separation levels, $k = 1, \cdots, 5$, and the second aircraft. The probabilities p_k by which the particles reach level k are given by Table 4 using Eq. (21).

$$p_k = \prod_{j=1}^{k} \gamma_j \tag{21}$$

Secondly, we simulate the situation that two aircraft conduct CDA operation using the ASAS speed control under the same condition for the first aircraft in the first simulation: a first aircraft enters IAF, then continuously descends to FAF by keeping a 2.5 degree flight path. After reaching the FAF at 2,000 ft, the aircraft reduces airspeed to 180 CAS knots and increases the flap angle to 25 degrees proportionally for 100 seconds. The second aircraft (a trailing aircraft) enters IAF 90 seconds after the first aircraft and trails the first aircraft (a target aircraft) while keeping 90 seconds separation. The ASAS spacing controller works to trail the target aircraft under the head-wind condition (section II B). The B747-400 dynamics are given to the two aircraft by AMAAI tool box. We use a computing time step of 0.1 second. For the initial deviation of altitude and CAS, Eqs. (17)-(20) and Table 2 are applied. By running ten times the IPS algorithm, the risk of the separation loss event is estimated. The number of particles per IPS simulation run is 10,000. For the ten IPS runs, the estimated fractions γ_k are given in Table 5 for

Table 3 Fractions γ_k of separation loss event in 90 seconds separation without ASAS

Separation level	1st IPS	2nd IPS	3rd IPS	4th IPS	5th IPS	6th IPS	7th IPS	8th IPS	9th IPS	10th IPS
1	1.0000	1.0000	1.0000	1.0000	1.0000	1.0000	1.0000	1.0000	1.0000	1.0000
2	0.9027	0.9024	0.9047	0.9054	0.9030	0.9035	0.9050	0.9075	0.9044	0.9039
3	0.2375	0.2433	0.2408	0.2317	0.2431	0.2413	0.2399	0.2322	0.2365	0.2429
4	0.0028	0.0073	0.0064	0.0035	0.0049	0.0068	0.0048	0.0030	0.0039	0.0048
5	0.0	0.0	0.0	0.0	0.0	0.0	0.0	0.0	0.0	0.0

Table 4 Probabilities p_k of separation loss event in 90 seconds separation without ASAS

Separation level	1st IPS	2nd IPS	3rd IPS	4th IPS	5th IPS	6th IPS	7th IPS	8th IPS	9th IPS	10th IPS	average	probability /flight hour
1	1.0000	1.0000	1.0000	1.0000	1.0000	1.0000	1.0000	1.0000	1.0000	1.0000	1.0000	1.0000
2	0.9027	0.9024	0.9047	0.9054	0.9030	0.9035	0.9050	0.9075	0.9044	0.9039	0.9043	1.0000
3	0.2144	0.2196	0.2179	0.2098	0.2195	0.2180	0.2171	0.2107	0.2139	0.2196	0.2160	0.6610
4	0.0006	0.0016	0.0014	0.0007	0.0011	0.0015	0.0010	0.0006	0.0008	0.0011	0.0010	0.0046
5	0.0	0.0	0.0	0.0	0.0	0.0	0.0	0.0	0.0	0.0	0.0	0.0

Table 5 Fractions γ_k of separation loss event in 90 seconds separation with ASAS

Separation level	1st IPS	2nd IPS	3rd IPS	4th IPS	5th IPS	6th IPS	7th IPS	8th IPS	9th IPS	10th IPS
1	1.0000	1.0000	1.0000	1.0000	1.0000	1.0000	1.0000	1.0000	1.0000	1.0000
2	1.0000	1.0000	1.0000	1.0000	1.0000	1.0000	1.0000	1.0000	1.0000	1.0000
2.1	0.0729	0.0691	0.0691	0.0707	0.0722	0.0694	0.0706	0.0711	0.0723	0.0721
2.2	0.0162	0.0166	0.01381	0.01424	0.01987	0.01780	0.01613	0.0153	0.01039	0.0193
3	0.0	0.0	0.0	0.0	0.0	0.0	0.0	0.0	0.0	0.0
4	0.0	0.0	0.0	0.0	0.0	0.0	0.0	0.0	0.0	0.0
5	0.0	0.0	0.0	0.0	0.0	0.0	0.0	0.0	0.0	0.0

Table 6 Probabilities p_k of separation loss event in 90 seconds separation with ASAS

Separation level	1st IPS	2nd IPS	3rd IPS	4th IPS	5th IPS	6th IPS	7th IPS	8th IPS	9th IPS	10th IPS	average	probability /flight hour
1	1.0000	1.0000	1.0000	1.0000	1.0000	1.0000	1.0000	1.0000	1.0000	1.0000	1.0000	1.0000
2	1.0000	1.0000	1.0000	1.0000	1.0000	1.0000	1.0000	1.0000	1.0000	1.0000	1.0000	1.0000
2.1	0.0729	0.0691	0.0691	0.0707	0.0722	0.0694	0.0706	0.0711	0.0723	0.0721	0.0710	0.2790
2.2	0.0012	0.0011	0.0010	0.0010	0.0014	0.0012	0.0011	0.0011	0.0008	0.0014	0.0011	0.0050
3	0.0	0.0	0.0	0.0	0.0	0.0	0.0	0.0	0.0	0.0	0.0	0.0
4	0.0	0.0	0.0	0.0	0.0	0.0	0.0	0.0	0.0	0.0	0.0	0.0
5	0.0	0.0	0.0	0.0	0.0	0.0	0.0	0.0	0.0	0.0	0.0	0.0

each of the separation levels and the second aircraft. Table 6 gives the probabilities p_k by which the particles reach level k using Eq. (21).

Figure 3 shows the simulation results shown in Table 4 and 6 for the comparison of the performance; the ASAS speed control is applied to the one, and not to the other. When the ASAS speed control is not applied to CDA operation, the level of the separation loss events gets higher than in the case when ASAS speed control is applied (Fig. 3). The MSI #2 (Table 1) probability is 66.10 %, and the Near Mid-Air Collision probability is 0.46%. This indicates that there are high chances that the ATCo instructs the trailing aircraft to control heading angle, speed, and/or maneuver out of the trail. On the other hand, the ASAS speed control works to keep the separation within MSI #2 in 90 seconds separation. This shows that the ASAS speed control is one of the positive applications to achieve CDA operation under the assumed condition. One may notice that Near Mid-Air and Mid-Air collision events are not yet counted in any of these simulations. This is in line with our prior expectations because our current SDCPN model does not yet cover rare non-nominal behaviors.
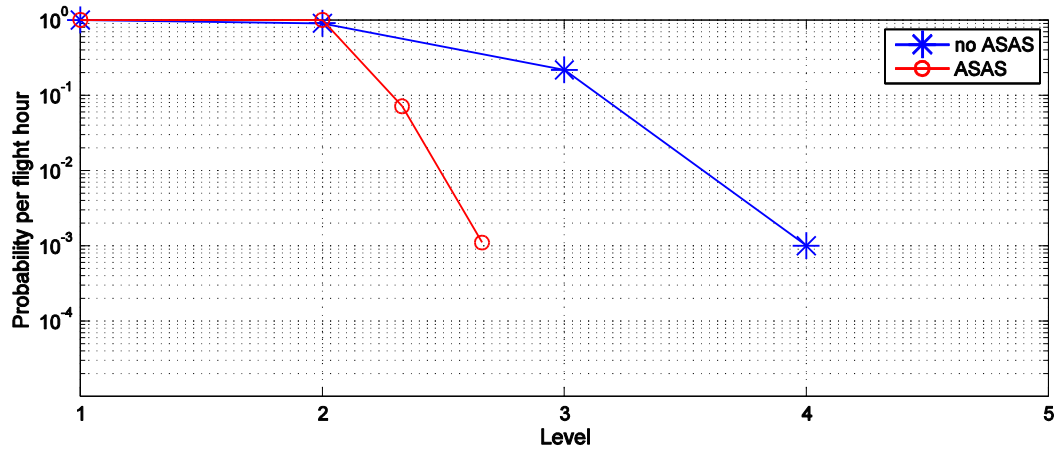
Fig. 3 Probabilities of the separation loss per flight hour: one applied ASAS, the other not

C. ASAS Speed Control Applied for Multiple Aircraft in In-trail Following

Next, the ASAS speed control is applied to multiple trailing aircraft under the same conditions with the two aircraft trailing in the previous section. By running twenty times the IPS algorithm, the risk of the separation loss event is estimated. The number of particles per IPS simulation run is 5,000.

The probabilities that the number 2, 3, 5, and 8 trailing aircraft reach the separation levels are shown in Table 7. Figure 4 plots the probabilities of Table 7. As shown in Table 7 and Fig. 4, the aircraft which reach MSI #2 are not counted in this simulation for all trailing aircraft. One of the reasons is that rare events, which cause critical operation, are not considered in this Monte Carlo simulation. Rare events which may break safety standards should be taken into account in the future based on this preliminary study. One of the interesting results here is that the separation performance is not deteriorated due to the increase in the number of the trailing aircraft. The performance of the ASAS spacing controller applied for multiple trailing aircraft was discussed in Ref. 4. Under the assumed condition, the ASAS speed control contributes well to conduct CDA operation for multiple trailing aircraft.

Table 7 Comparison of probability of separation loss event for multiple aircraft

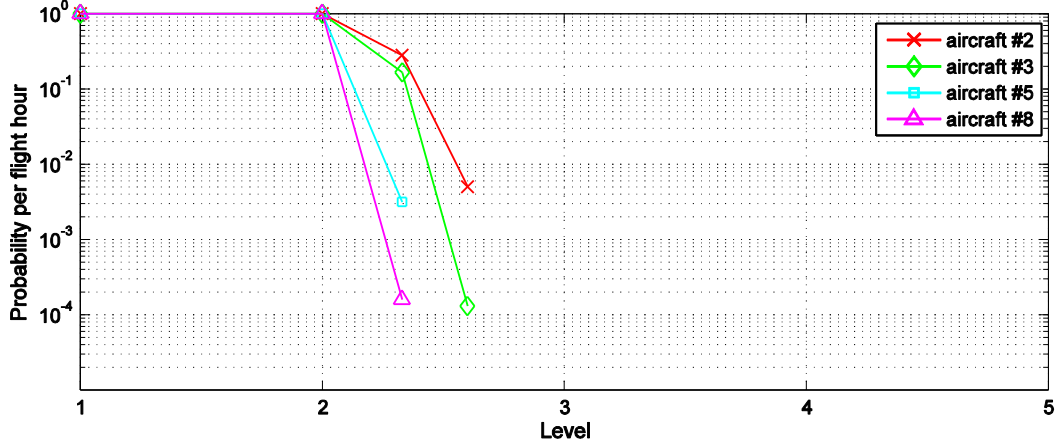| Separation level	Aircraft #2	Aircraft #3	Aircraft #5	Aircraft #8
1	1.0	1.0	1.0	1.0
2	1.0	1.0	1.0	1.0
2.1	0.27897	0.16542	0.00315	0.00016
2.2	0.00503	0.00013	0.0	0.0
3	0.0	0.0	0.0	0.0
4	0.0	0.0	0.0	0.0
5	0.0	0.0	0.0	0.0

Fig. 4 Probabilities of the separation loss per flight hour: Applied ASAS speed control to multiple trailing aircraft

V. Concluding Remarks

This paper confirmed the performance of the ASAS speed control applied for CDA operation. The ASAS control loop was modeled using SDCPN. Based on the designed SDCPN models, Monte Carlo simulations were run to count the separation loss events. Stochastic behaviors of multiple aircraft and wind speed which depends on aircraft altitude were considered in the simulation. The results of the Monte Carlo simulations showed probabilities of separation loss events. It was indicated that the ASAS speed control was one of the positive applications for CDA operation under the nominal condition. One of the interesting results was that the separation performance was not deteriorated due to the increase in the number of trailing aircraft under the simulated condition.

The novelty of this study over the preceding study[3] is that serious disturbances and multiple aircraft have been considered, for which ASAS spacing still works well thanks to the novel controller in Ref. 4. The preceding study analyzed that starting the ASAS spacing with initial speed deviation triggered strong acceleration and higher speed of aircraft, and this caused critical separation loss events in two aircraft trailing. However, this research confirmed that the ASAS spacing worked well when the novel controller was applied under the initial speed and altitude deviation, not only for two aircraft trailing, but also for multiple aircraft trailing.

Based on this preliminary study in ASAS control, this research is going to develop the SDCPN models and Monte Carlo simulation study for safety/performance analysis including rare events, for example, hardware failures and human performances. We are going to compare the simulation results with these of the past study to confirm how the improvement in the current study works under the effects of rare events. This paper only takes into account speed control. Hence vectoring approaches should be considered in S&M scenarios. Our approach will be further developed for evaluation of the future S&M operation.

Appendix

A. Aircraft Dynamics[8]
Aircraft state variable $\boldsymbol{y}$ is

$$\boldsymbol{y} = \int \dot{\boldsymbol{y}} dt \qquad (A1)$$

$$\begin{aligned}
\dot{\boldsymbol{y}} &= f(\boldsymbol{y}, \ \boldsymbol{u}, \ \boldsymbol{\omega}) \\
&= [\dot{y}_1, \ \dot{y}_2, \ \dot{y}_3, \ \dot{y}_4, \ \dot{y}_5, \ \dot{y}_6, \ \dot{y}_7, \ \dot{y}_8]^T \\
&= [\dot{x}_{east}, \ \dot{x}_{north}, \ \dot{h}, \ \dot{V}, \ \dot{\gamma}, \ \dot{\varphi}, \ \dot{\psi}, \ \dot{m}]^T
\end{aligned} \qquad (A2)$$

$$\dot{x}_{east} = V \cos\gamma \ \sin\psi + \omega_x \qquad (A3)$$
$$\dot{x}_{north} = V \cos\gamma \ \cos\psi + \omega_y \qquad (A4)$$
$$\dot{h} = V \ \sin\gamma + \omega_z \qquad (A5)$$
$$\dot{V} = \frac{T \ \cos\alpha - D}{m} - g \sin\gamma \qquad (A6)$$

$$\dot{\gamma} = \frac{L+T\sin\alpha}{mV}\cos\varphi - \frac{g}{V}\cos\gamma \tag{A7}$$

$$\dot{\varphi} = p \tag{A8}$$

$$\dot{\psi} = \frac{g\,\tan\varphi}{V} \tag{A9}$$

$$\dot{m} = -Q \tag{A10}$$

Here

x_{east}	: aircraft position on x axis, positive value to the east direction
x_{north}	: aircraft position on y axis, positive value to the north direction
h	: aircraft position on z axis (altitude)
V	: aircraft true air speed (TAS)
γ	: vertical flight path angle
φ	: roll angle (bank angle)
ψ	: yow angle (heading angle)
m	: aircraft mass
ω_x	: wind component on x axis
ω_y	: wind component on y axis
ω_z	: wind component on z axis
T	: thrust
D	: drag
L	: lift
α	: angle of attack
g	: gravity
Q	: fuel consumption

Lift L is:

$$L = \frac{1}{2}\rho V^2 C_L\ S \tag{A11}$$

Lift coefficient C_L is:

$$C_L = C_{L0} + C_{L\alpha}\ \alpha \tag{A12}$$

Here

ρ	: air density
S	: wing area
C_{L0}	: function of flap deflection
$C_{L\alpha}$	: lift curve slope

$S, C_{L0}, C_{L\alpha}$ are given by AMAAI tool box.

Drag D is:

$$D = \frac{1}{2}\rho V^2 C_D\ S \tag{A13}$$

Drag coefficient C_D is:

$$C_D = C_{D0} + kC_L^2 + \Delta C_{D_{flaps}} + \Delta C_{D_{mach}} + \Delta C_{D_{gear}} \tag{A14}$$

Here

C_{D0}	: coefficient of zero-lift drag
k	: proportional constant in induced drag term
$C_{D_{flaps}}$	: coefficient of the drag due to flap extension
$C_{D_{mach}}$	: coefficient of mach-rise component
$C_{D_{gear}}$	: coefficient of gear change

$C_{D0}, k, C_{D_{flaps}}, C_{D_{mach}}, C_{D_{gear}}$ are given by AMAAI tool box[8].

B. TECS[12]

Thrust command T_{cmd} and pitch command θ_{cmd} are given by:

$$T_{cmd} = \left[\frac{K_{TI}}{s}\left\{(\gamma_{cmd} - \gamma) + \left(\frac{\dot{V}_{cmd}}{g} - \frac{\dot{V}}{g}\right)\right\} + K_{TP}\left(\gamma - \frac{\dot{V}}{g}\right)\right] m \qquad (A15)$$

$$\theta_{cmd} = \frac{K_{EI}}{s}\left\{\left(\frac{\dot{V}_{cmd}}{g} - \frac{\dot{V}}{g}\right) - (\gamma_{cmd} - \gamma)\right\} + K_{EP}\left\{(2 - K)\gamma - K\left(\frac{\dot{V}}{g}\right)\right\} \qquad (A16)$$

K_{TI} : gain in TECS (Total Energy Control System)
K_{TP} : gain in TECS
K_{EI} : gain in TECS
K_{EP} : gain in TECS
K : gain in TECS
s : Laplace transform

C. Aircraft Guidance Behavior

Figure A1 shows the SDCPN model for Aircraft guidance behavior model. The model consists of two places; Descent and Level. The token firstly resides at the place, Descent. While the token is at Descent, the aircraft descends to altitude 2,000 ft using automatic speed control in CDA operation. After reaching the altitude, the token moves to the place Level. The aircraft starts level flight by automatic speed control. The token includes dynamics of six degrees-of-freedom axis aircraft model and autopilot model designed by Total Energy Control System (TECS)[12] in the token color functions. The dynamics models are described in Appendix A and B.
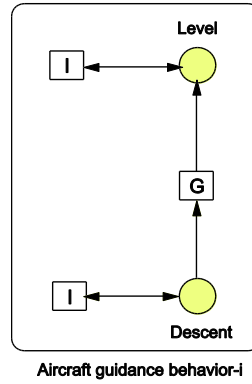

Fig. A1 Aircraft guidance behavior Petri net model

Figure A2 shows interactions of the Aircraft guidance behavior model. Four incoming arcs and two arrows are from Aircraft air data PROC, Aircraft horizontal POS-PROC, FMS flight plan, Wind model, and ASAS spacing model. They show the following information flow from the other models:

Incoming from Aircraft air data PROC
ϵ_z : position error on z axis
v_z : velocity error on z axis
v_{TAS} : TAS error

Incoming from Aircraft horizontal POS-PROC
ϵ_x : position error on x axis
ϵ_y : position error on y axis
v_x : velocity error on x axis
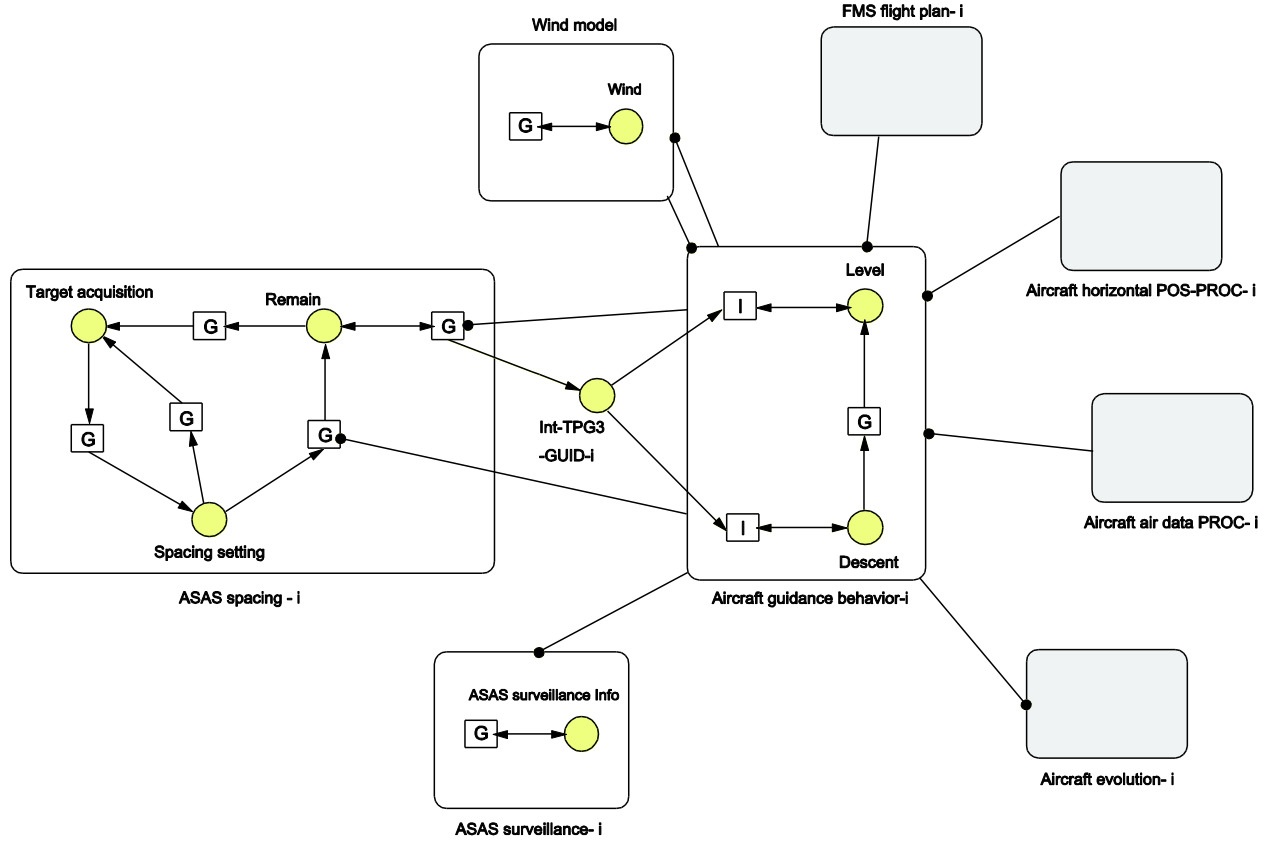v_y : velocity error on y axis

Fig. A2 Interactions for Aircraft guidance behavior

Incoming from FMS flight plan

x_{IAF} : IAF position on x axis
y_{IAF} : IAF position on y axis
x_{FAF} : FAF position on x axis
y_{FAF} : FAF position on y axis

Incoming from Wind model

ω_x : wind speed on x axis
ω_y : wind speed on y axis
ω_z : wind speed on z axis

Incoming from ASAS spacing

V_{cmd} : TAS speed command

The above incoming information is used in token color functions and transition of the state, Descent and Level. How this information contributes in the aircraft model and TECS is shown in Appendix A and B. The atmospheric conditions (wind and disturbance) in the Wind model LPN is shown in section II. B.

American Institute of Aeronautics and Astronautics
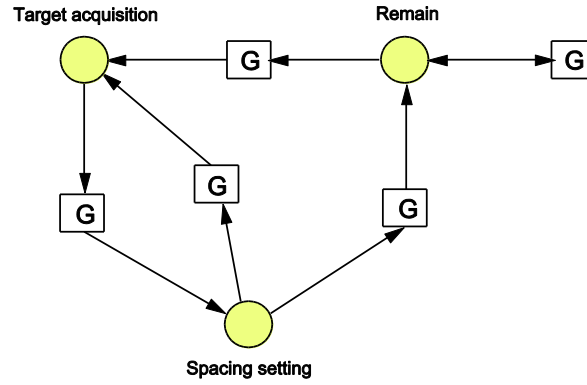
D. ASAS Spacing

Fig. A3 ASAS spacing Petri net model

Figure A3 shows the SDCPN model which represents the ASAS spacing model. The ASAS spacing model consists of three places; Target acquisition, Spacing setting, and Remain. When the token resides at Target acquisition, a target aircraft is selected. Spacing setting gives desired spacing time. At Remain, the ASAS space keeping controller works to keep the desired spacing time. If the selected target aircraft is not included in ADS-B range, then the token moves to Target acquisition from both Remain and Spacing setting. If the target aircraft is included, the token moves from Target acquisition to Spacing setting, and then to Remain.
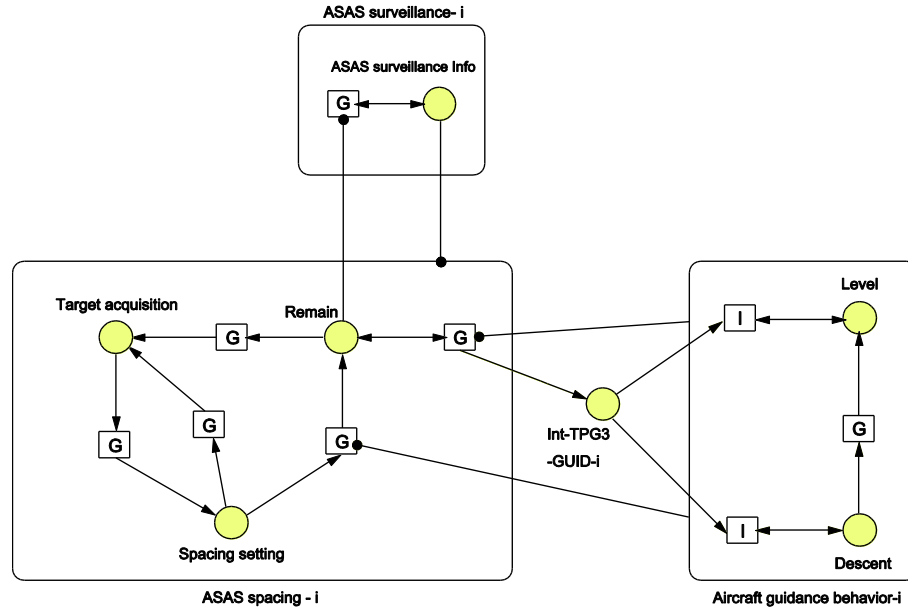

Fig. A4 Interactions for ASAS spacing

Figure A4 shows interactions of the ASAS spacing model. Two incoming arcs are from ASAS surveillance and Aircraft guidance behavior model. The following information is given to ASAS spacing model from ASAS surveillance and Aircraft guidance behavior model:

Incoming from ASAS surveillance

Q : Call signs of all aircraft in ADS-B range

q_{target} : Call sign of a target aircraft

$\hat{x}_1^{lead}$: x axis position of a lead (target) aircraft, positive value is given to the east direction.

$\hat{x}_2^{lead}$: y axis position of a lead (target) aircraft, positive value is given to the north direction.

V_{GS}^{lead} : Ground speed of a lead (target) aircraft

Incoming from Aircraft guidance behavior

$\hat{x}_1^{own}$: x axis position of an own (trailing) aircraft, positive value is given to the east direction.

$\hat{x}_2^{own}$: y axis position of an own (trailing) aircraft, positive value is given to the north direction.

V_{GS}^{own} : Ground speed of an own (trailing) aircraft

Using the above incoming information, an airspeed command which achieves the desired time spacing between a target aircraft and an own aircraft is calculated in the token color function. The speed control algorithm is shown in section II. A. The airspeed command is input to autopilot in the Aircraft guidance behavior model.

References

[1]Package I Requirements Focus Group (RFG) Application Definition Sub-group, "Package I: Enhanced Sequencing and Merging Operations (ASPA-S&M) Application Definition", 2.3.0 ed., January 20, 2009.

[2]Shah, A.P., Pritchett, A.R., Feigh, K.M., Kalarev, S.A., Jadhav, A., Corker, K.M., Holl, D.M., and Bea, R.C., "Analyzing Air Traffic Management Systems using Agent Based Modeling and Simulation", *Proc. 6th USA/Europe ATM R&D Seminar*, 2005.

[3]Oliveira, I. R., Blom, H. A. P., and Bakker, G. J., "Modeling and Estimation of Separation Criteria for Airborne Time-Based Spacing Operation", *Proc. 7th USA/Europe Air Traffic Management R&D Seminar*, 2007.

[4]Itoh, E., Van der Geest, P. J., and Blom, H., "Improved Airborne Spacing Control for Trailing Aircraft", *Proc.2009 Asia-Pacific International Symposium on Aerospace Technology*, 2009

[5]Everdij, M.H.C., Klompstra, M.B., Blom, H.A.P., and Klein Obbink, B., "Compositional specification of a multi-agent system by stochastically and dynamically coloured Petri nets, In: H.A.P. Blom, J. Lygeros (eds.), Stochastic hybrid systems: Theory and safety critical applications", Springer, pp. 325-350, 2006.

[6]Everdij, M.H.C., Bakker, G.J., Blom, H.A.P., EMERTA WP3.2, "Safety/separation modelling of a particular ASAS application", *EMERTA/WP3.2/NLR/MAIN/2.0, Version 2.0*, 2001

[7] Blom, H.A.P., Krystul, J., Bakker, G.J., Klompstra, M.B., and Klein Obbink B., "Free flight collision risk estimation by sequential Monte Carlo simulation, Eds: C.G. Cassandras and J. Lygeros, Eds: Stochastic hybrid systems; recent developments and research trends", Taylor & Francis/CRC Press, chapter 10, pp. 249-281, 2007.

[8]Van der Geest, P. J., "The AMAAI Modeling Toolset for The Analysis of In-trail Following Dynamics, Deliverable D2: Description and User Guide", *NLR-CR-2002-112*, 2002.

[9]CoSpace, http://www.eurocontrol.int/eec/public/standard_page/SSP_cospace_home.html

[10]European Aviation Safety Agency, "Decision No. 2003/6/RM of the Executive Director of the Agency: On Certification Specifications, Including Airworthiness Codes and Acceptable Means of Compliance, for All Weather Operations (CS-AWO)", 2003.

[11]Military Specification, "Flying Qualities of Piloted Airplanes", *MIL-F-8785C*, 1980.

[12]Lambregts, A. A., "Automatic Flight Controls: Concepts and Methods", *FAA report*, 1998.